POLİTEKNİK DERGİSİ

JOURNAL of POLYTECHNIC

ISSN: 1302-0900 (PRINT), ISSN: 2147-9429 (ONLINE)
URL: http://dergipark.org.tr/politeknik

Finite element analysis of the inductance and magnetic field in the permanent magnet spherical motor

Yazar(lar) (Author(s)): *Sibel AKKAYA OY[1], Osman GÜRDAL[2], Serdal ARSLAN[3]*

ORCID[1]: 0000-0002-1209-920X

ORCID[2]: 0000-0001-8315-7342

ORCID[3]: 0000-0002-1187-5633

Bu makaleye şu şekilde atıfta bulunabilirsiniz(To cite to this article): Akkaya Oy S., Gürdal S., Arslan S., "Finite element analysis of the ınductance and magnetic field in the permanent magnet spherical motor", ***Politeknik Dergisi***, 23(4): 1387-1394, (2020).

Erişim linki (To link to this article): http://dergipark.org.tr/politeknik/archive

DOI: **10.2339/politeknik.597962**

Finite Element Analysis of the Inductance and Magnetic Field in the Permanent Magnet Spherical Motor

Highlights

- *Spherical motor's windings*
- *Mutual inductance*
- *Self inductance*
- *Curve fitting method*
- *Torque change*

Graphical Abstract

In this study, an air core spherical motor which has rotor and stator winding arrangement is described.

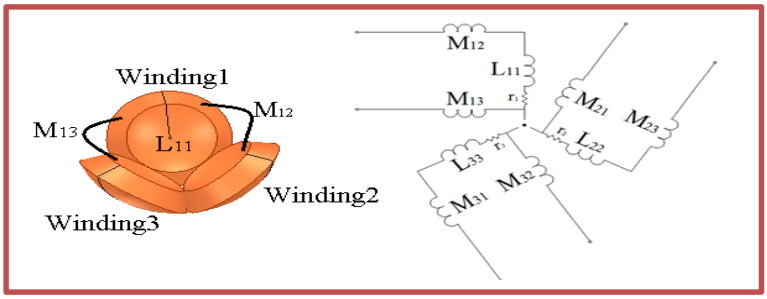

Figure. Winding inductance relationship and equivalent circuit model

Aim

Mutual inductance and self-inductance change were examined according to r=4, 20, 40 and 60 mm radius and the change in the number of stator winding for the spherical motor.

Design & Methodology

Stator poles on the stator were placed at specified angles. Stator poles were placed with an angle of 45° to x axis and with an angle of 120° to z axis.

Originality

It has never worked in the literature with a spherical motor of this size before.

Findings

This study examined mutual inductance and self-inductance change according to r=4, 20, 40 and 60 mm radius and the change in the number of coils for a spherical motor. Changes in inductance were found through curve fitting method with the coefficients of cubic equations.

Conclusion

With the change of size (scale change) in the analyzed spherical motor, the torque increases, but the torque density decreases.

Declaration of Ethical Standards

The authors of this article declare that the materials and methods used in this study do not require ethical committee permission and/or legal-special permission.

Finite Element Analysis of the Inductance and Magnetic Field in the Permanent Magnet Spherical Motor

Araştırma Makalesi / Research Article

Sibel AKKAYA OY[1]*, Osman GÜRDAL[2], Serdal ARSLAN[3]

[1]Marine Science and Technology Engineering, Faculty of Marine Sciences, Ordu University, Turkey,
[2]Department of Electrical Engineering, Faculty of Technology, Gazi University, Turkey
[3]Birecik Vocational Higher School, Harran University, Şanlıurfa, Turkey
(Geliş/Received :29.04.2019 ; Kabul/Accepted : 29.04.2020)

ABSTRACT

Today, many applications requiring mass manufacturing are shifting to robotic applications through automation systems. The actuators used in these robotic systems should be designed according to needs. In this study, an air core spherical motor which has rotor and stator winding arrangement is described. The spherical motor's windings are optimally positioned on the stator made of delrin. Mutual inductance and self-inductance change were examined according to r=4, 20, 40 and 60 mm radius and the change in the number of stator winding for the spherical motor. Changes in inductance were found through curve fitting method with the coefficients of cubic equations. Equivalent circuit with winding inductance model is also given. Torque change according to magnet change was also investigated. Magnetic flux density change of N52 M magnet 3 winding 2-pole model was examined and the effect of the increase in overall size on torque was evaluated.

Anahtar Kelimeler: Spherical motor, curve fitting, permanent magnet, torque.

1. INTRODUCTION

In industrial and robotic applications, multi-free rotational motion is very important. While normal electrical motors can rotate around a fixed axis, spherical motor can rotate every direction around a specific point. This way, it has an important advantage over electric motors which can rotate. A spherical actuator has a compact structure, high energy density, low moment of inertia and rapid response[1]. The spherical motors are used in security and personal cameras, articulation points of robots, laser cutters, telescopes, solar panels, exoskeletons and applications which require multi-axis motion. It has even been considered to be used as energy harvester [2] and generator [3] recently.

As is known, the first examples of application on spherical machines are induction motor simulations in terms of working principles. Diversification of magnet materials over time has led to the development of permanent magnet spherical motors. Magnet array of other permanent motors (Halbach array [4,5], surface magnet radial array [6-10] and axial array [11-13]) can also be adapted to these motors. Rotors of permanent

magnet spherical motors are also spherical. When the spherical motors' degree of freedom of movement is considered, 3D analysis method is required instead of 2D numerical analysis method. In particular, 2D analysis can be performed with the spherical motor simulation of rotor surface radial flux motor [9-10]. Xia et al. proposed the torque calculation method based on the 2-D conversion model in order to avoid the complicated torque calculation process under 3-D magnetic field and thus reduce the computational burden and it was found that the torque values of the model proposed which was transformed to 2D from 3D were very close to each other [14]. Magnet can be combined in different ways to acquire the shape of sphere. Air gap flux density, size and wave form can vary. According to obtaining a spherical rotor by increasing the number of magnets in the form of pieces rotor position change, magnetic flux can approache sinusoidal wave [15]. However, due to high magnet costs, application of special magnet shapes can increase production costs [15]. Considering torque equality [16]; the amount and change of flux density in air gap is important according to position change of the motors. In addition, the type of magnet on the rotor affects torque size of the motor significantly [17]. Zhang [8] analyzed the air core 24/8 spherical motor using the finite element method. By using the finite element method, the magnet thickness and air gap change of spherical motor torque [18]. Qian et al. [19] showed that axial magnet array showed higher flux density than radial array. Using iron core can produce about 4.9 times more torque when compared with air core. The increase in the air gap between stator and rotor linearly decreases the produced torque significantly. In addition, they showed that maximum torque was close to each other in the same ampere winding and volume between cylindrical magnet and conic magnet (with cylindrical magnets of different diameters in a row) of rotor magnet geometry [19]. For this reason, studies on spherical motors with cylindrical magnets on rotor surfaces have increased recently in terms of ease of production.

*Sorumlu yazar(Corresponding Author)
e-posta : sibelakkayaoy@gmail.com

With each current pulse of the spherical motor, the shaft of the motor moves by an angle. The current pulses sent to the motor must be in a certain order considering the rotation axis. As is known, each motor winding has a certain inductance and resistance value. Since the stator windings contain inductance and resistance, the Is current echospotically increases with the L / R time constant of the winding. In general, smaller motors rotate faster due to low inductance and low rotor inertia. At higher rotational speeds, torque drop may occur because the winding inductance limits the rate of change of the current, so that the current cannot reach its full value at each step. Most of the studies in literature have focused on magnetic flux density, torque change and control in addition to traditional and new spherical motor studies.

It is very important to determine the parameters of permanent magnet motors. Especially motor parameter changes can cause incorrect determination of rotor and speed position in sensorless control methods and incorrect determination of motor flux in direct moment control [20]. For parameter estimation of permanent magnet motors, extended kalman filter [21], recursive least squares method [22], model reference adaptive system [23], finite elements method, artificial neural networks [24] and adaptive prediction methods [25] have been proposed.

Since magnetic flux primariy flows through the iron core with high permeability, a core-type spherical motor shows the advantage of low-leakage magnetic flux. On the contrary, because of not having an iron core within the winding, this slotless spherical motor has the disadvantage of a high leakage of magnetic flux. However, considering the absence of a reluctance difference between the stator and rotor, this motor has the advantage of position control [26].

Akkaya proposed a slotless spherical motor model with a two-pole permanent magnet rotor of 8 mm diameter and a stator consisting of 3 independent windings [16,27]. By examining the results of analytical and numerical analysis on the engine, he stated in the experimental study that 360 ° rotation freedom was obtained in the z axis and 44 ° rotation freedom was obtained upward-downward. In another study [27], she compared the torque size analytical and simulation results of a three-coil spherical motor. This study examined mutual inductance and self-inductance change according to r=4, 20, 40 and 60 mm radius and the change in the number of coils for a spherical motor. Changes in inductance were found through curve fitting method with the coefficients of cubic equations. In this context, first the structure of the spherical motor was introduced, and then numerical analysis was performed with Ansys Maxwell 3D software. Magnetic flux and torque changes were investigated. Basic equations were given for inductance calculations. Inductance change was examined in section 3. Finally, the results were evaluated in the last section.

2. DESIGN AND MATERIALS

Stator poles on the stator were placed at specified angles. Stator poles were placed with an angle of 45° to x axis and with an angle of 120° to z axis. Figure 1 shows the windings at the designed stator.

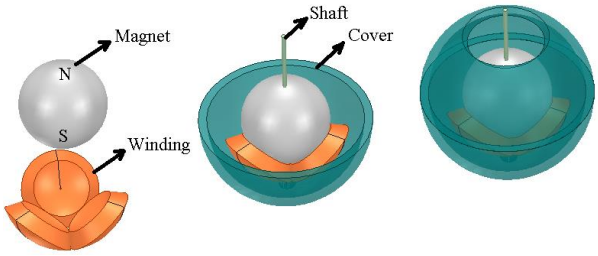

(a)

(b)

Figure 1. a) Designed stator, windings and general appearance of the spherical motor, b)Prototype motor

By designing stator windings spherically, the aim was to use the structure of the spherical actuator in the most effective way.

Table 1. The properties of this model

Properties	Value
The number of stator windings	3
The number of rotor poles	2
Stator radius	5.7 (mm)
Rotor radius	4 (mm)

Figure 2 shows the air core winding used in spherical actuator/motor. R0 is the radius of rotor, R1 is the distance of the inner surface of winding to the centre, R2 is the distance of the outer surface of winding to the centre, ζ0 is the angular diameter of air core, and ζ1 is the angular diameter of winding [28,29].

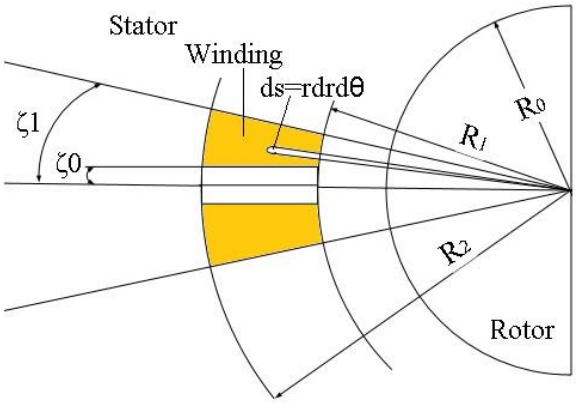

Figure 2. Winding with air core winding.

Stator winding lenght;

$$Lc = R2 - R1 \quad (1)$$

According to the winding parameters given in Figure 2, since the amount of amperage increases in constant current as small ζ_1 angle of the ζ_0 angle enlarges, torque will increase. Similarly, with the outer diameter increasing as the inner diameter remains constant, the torque size will increase. However, decreasing flux amount as it moves away from the rotor limits the length of the outer diameter of the winding. Similarly, increasing the inner angle by considering the outer angle of the winding constant decreases the torque magnitude [17].

Eq. 2 was used to find out the physical rotation capacity of the rotor based on the stator winding numbers of stator. This rotation capacity expresses the angle of rotor shaft touching the windings. Here, θ=135°.

$$\theta_r = \theta - \zeta_1 \quad (2)$$

Table 2. Changes in winding outer angle and movement angle according to the number of windings

Number of windings	Winding outer angle	Movement angle
6	20,7°	114,3°
5	24,55°	110,45°
4	30°	105°
3	37,76	97,24°
2	45°	90°

3. FINITE ELEMENTS MODEL

With the complexity of the spherical motor structure and the difficulty of analytical calculation, in order to obtain more accurate results, the finite element method (FEM) is widely used in the analysis of the electromagnetic characteristics of the motor.

In Ansys Maxwell, which is widely preferred in the literature, first the dimension to be designed for machine geometry is selected. Machine geometry is created according to the calculated geometry data. Magnetostatic analysis is selected for the drawn model. As model parameters; the boundary conditions are given in AmperTurn (Figure 3). The designed machine is made ready for analysis. Although it may seem small in the program algorithm, Mesh identification is very important for the machine to provide sufficient solution. Unknown magnitudes (potential, electric field,…) in each network region are represented by scalar or vectorial partial differential equations. Therefore, increasing the number of networks increases the accuracy of the obtained sizes. According to the analysis algorithm, first the system to be modeled is divided into four-sided elements and a finite element network is formed (Figure 3). During the solution process, networks are improved through iterations and errors are reduced. Before starting the field solution, the conduction current in the conductors is simulated and the field solution starts. The magnetic field strength (H) at the midpoints of the edges of each four-sided element in the finite element network is calculated by using the current density. In case of the magnetic core material not being linear, the Newton-Raphson method uses magnetic field strength. In addition, the B-H curve of the material is used to solve a nonlinear problem with a linear approach. With this approach, close results are obtained for the nonlinear solution of H. The solver writes down the completed solution in a file and performs error analysis. With adaptive analysis, the solver minimizes the faultiest quadratic elements and continues the solution until the specified error criterion is met. As a result, inductance values are calculated, current density, magnetic field strength, magnetic flux density and forces are obtained [30]. Since the spherical motor has three-dimensional geometry, 3D simulations require a large amount of computing time [31].

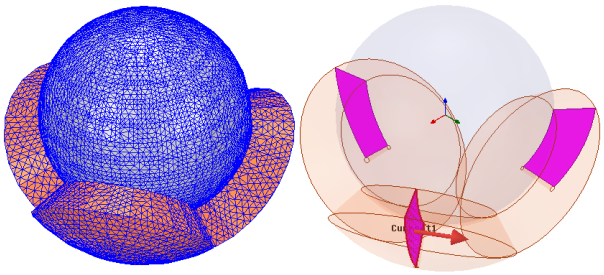

Figure 3. Mesh structure and excitation current

Total number of elements is 168131. Winding excitation currents are shown. The finite element analysis software is used to calculate the magnetic field and torque of the motor. Under the condition of steady magnetic field, the Maxwell equation is:

$$\nabla \times H(x,y,z) = J(x,y,z) \quad (3)$$

$$\nabla . B(x,y,z) = 0 \quad (4)$$

In order to obtain the value of flux density components in the spherical coordinate system, conversion is made from the cartesian coordinate system (Equation 5).

$$\begin{matrix} B_{lr} \\ B_{l\theta} \\ B_{l\varphi} \end{matrix} = \begin{bmatrix} sin\theta cos\emptyset & sin\theta sin\emptyset & cos\theta \\ cos\theta cos\emptyset & cos\theta sin\emptyset & -sin\theta \\ -sin\emptyset & cos\emptyset & 0 \end{bmatrix} \begin{bmatrix} B_x \\ B_y \\ B_z \end{bmatrix} \quad (5)$$

where r, θ, φ are the three components of the air-gap flux density in the spherical coordinate system.

Lorentz force law is very useful if there is a torque or force generated by a conductor carrying current in a magnetic field produced by a permanent magnet.

$$dF = I_w dl \times B \quad (6)$$

In Eq. 6, dl is the differential length of the part. A torque is generated on the rotor due to the interaction between the stator windings passing through it and the magnetic field of the rotor [32].

$$T = -\int_v r(J.B)dv \quad (7)$$

Here; v is the volume of the conductor carrying the current. According to torque equation given in Eq. 8, torque size is influenced by the changes in size given in Figure 2. If integral is taken over the entire winding volume, the torque equation is written as in eq. 5[16-17,27].

$$T_c = -J\int_{R_1}^{R_2}\int_{\zeta_0}^{\zeta_1}\left\{\int_c rB_{Ir}(r,\theta,\phi)dl\right\}rdrd\zeta \quad (8)$$

Here $B_{Ir}(r,\theta,\phi)$ is the magnetic flux density in spherical coordinates and J is the flux density. As shown in Equation 8; torque is influenced by current, magnetic flux density and winding dimensions. Although there is sufficient amperage to the windings, the characteristic of the magnet material changes the torque size. Using NdFeB35 or SmCo28 permanent magnets in rotor structure of spherical motor would increase torque and power density values up [33]. NdFeB52 magnet which have the best performance permanent magnets with 406 kJ/m^3 maximum energy multiply are made by Neodymium-Ferrite-Boron material [34]. For this reason, torque variation was investigated for NdFeB type materials.

3.1. Torque Change of Magnet Change

In Figures 4 and 5, torque was examined according to exchange of NdFeB type magnets and Ansys Maxwell 3D model with continuous state analysis.

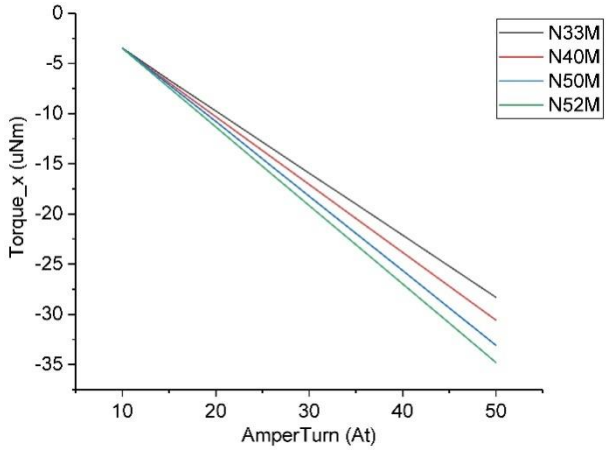

Figure 4. Torque change in x component according to magnet types

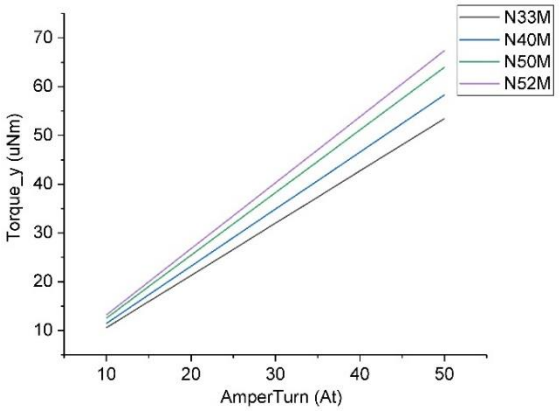

Figure 5. Torque change in y component according to magnet types

As a result of the excitation current applied to the winding, x and y rotate in their axis. The torque increased linearly as the magnet flux density increased. The Residual Flux Density (Br) of the N52M is 1.3063 T, while the N33M Br is 1.034 T. The Br value of N52M magnet is higher than other magnet types. As shown in Figures 4 and 5, the torque value increased by the amount of Br increase.

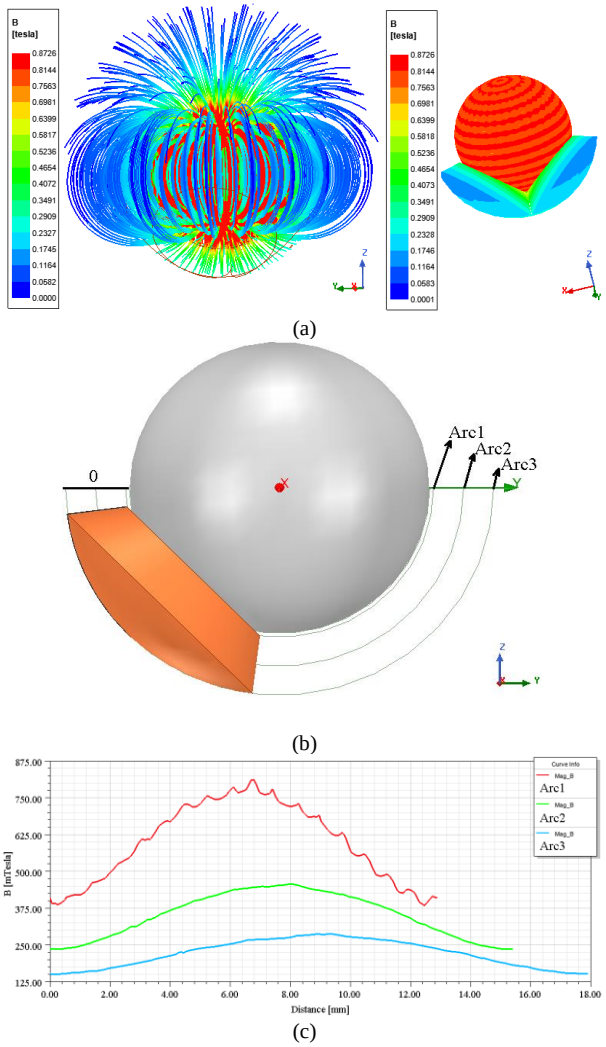

Figure 6. a) Model magnetic flux density distribution, b) Display of springs along the single winding of the model, c) Magnetic field change along the springs

As shown in Figure 6, the distribution of the area is uniform due to the air core. The area density in the winding surface region is about 0.8 T. The increase in the field distribution as the magnet approaches and the decrease in the points where the polarity changes are the expected results. Flux density decreased approximately twice as the polarity shift limit was approached. The torque change according to the increase in the size of the spherical motor is examined in Figure 7. Scale 1 here is the size of the model that is discussed and prototyped. Scale increase is in the form of dimension-fold.

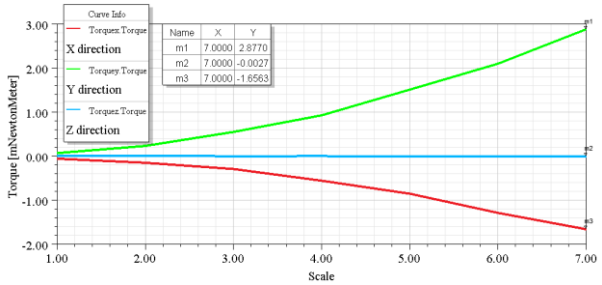

Figure 7. Torque change according to total size ratio change

When the scale is 1, the outer radius is 5.7 mm and when the scale is 7, the outer radius is 39.9 mm. Since no change in flux density is observed as the scale increases, it was not given in a graph. However, according to the calculations, the torque per volume (Torque / Volume) decreases as the scale ratio increases. This has to be taken into consideration when designing permanent magnet spherical motors in large diameters.

3.2. Analysis of Spherical Motor Inductance Changes

Magnetostatic solver gives inductance and coupling values in matrix form. As is known, inductance is the difficulty of flux against the change of time. The inductance matrix shows the relationship between current and total flux for three independent current cycles. Let's consider three windings placed on the sphere in Figure 8a. The axes of the coils passing through the center of the sphere, the currents passing through winding 1, winding 2 and winding 3 will affect each other. This interaction between coils is called mutual inductance. Figure 8b shows the inductance and mutual inductance of three winding with 120° difference between and equivalent circuit.

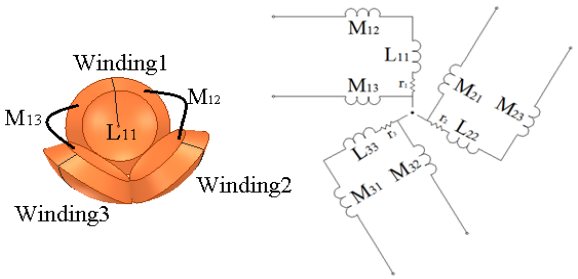

Figure 8. Winding inductance relationship and equivalent circuit model

The rate of change in the flux of circle per unit change in the current is called the inductance of winding [35]. We can show the inductance of first winding with L11, the mutual inductance of the first winding due to the flux generated by the second winding with M12 and the mutual inductance of the first winding due to the flux generated by the third winding with M13. Self inductance and mutual inductance values for rotor diameters of different values for two-winding, three-winding, four-winding, five-winding and six-winding were found by using Ansoft (Ansys) Maxwell 3D. Self-inductance curve for r=4, 20, 40 and 60 mm radius in terms of the number of winding is shown in Figure 9.

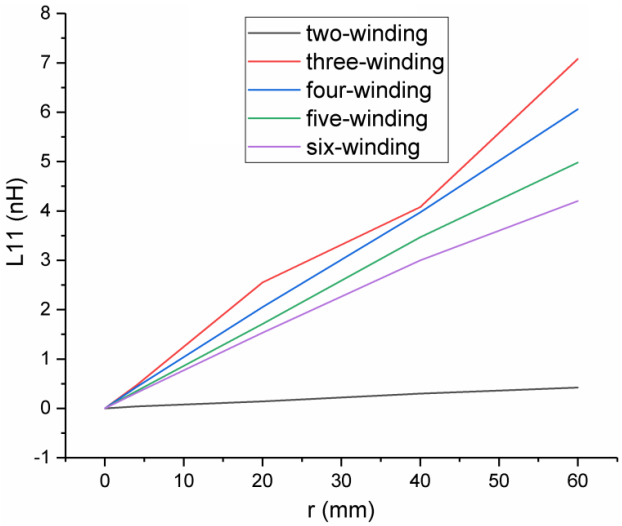

Figure 9. Self-inductance graph of the first winding for the number of winding

As can be seen in Figure 9, as the radius length of the spherical motor increases, self inductance also increases. Each winding inductance change was examined to be able to estimate inductance values of different radius. According to this graph, separate curve fitting processes were conducted according to L11 self-inductance value found as a result of analysis. According to the result of this operation, inductance equation was written down by using f(x) function. These functions are given in Eq. 9.

$$f(x) = p_1 x^3 + p_2 x^2 + p_3 x + p_4 \quad (9)$$

Here, p1, p2, p3 and p4 constants. x expresses r radius.

Table 3. Function coefficients according to the number of winding

Number of winding	F(x)	Self-inductance
2	$p_1 = -4{,}971 \times 10^{-5}$ $p_2 = 0{,}004565$ $p_3 = 0{,}03331$ $p_4 = 0{,}5882$	L_{11}
3	$p_1 = 5{,}947 \times 10^{-5}$ $p_2 = -0{,}005296$ $p_3 = 0{,}2276$ $p_4 = -0{,}3573$	L_{11}
4	$p_1 = 6{,}667 \times 10^{-6}$ $p_2 = -0{,}000586$ $p_3 = 0{,}1124$ $p_4 = -0{,}007806$	L_{11}
5	$p_1 = -6{,}906 \times 10^{-6}$ $p_2 = 0{,}000518$ $p_3 = 0{,}07614$ $p_4 = 0{,}03868$	L_{11}
6	$p_1 = -4{,}595 \times 10^{-6}$ $p_2 = 0{,}0002184$ $p_3 = 0{,}07316$ $p_4 = 0{,}01948$	L_{11}

Figure 10-11 shows the mutual inductance curve according to two and three-winding and for r=4, 20, 40 and 60 mm radius.

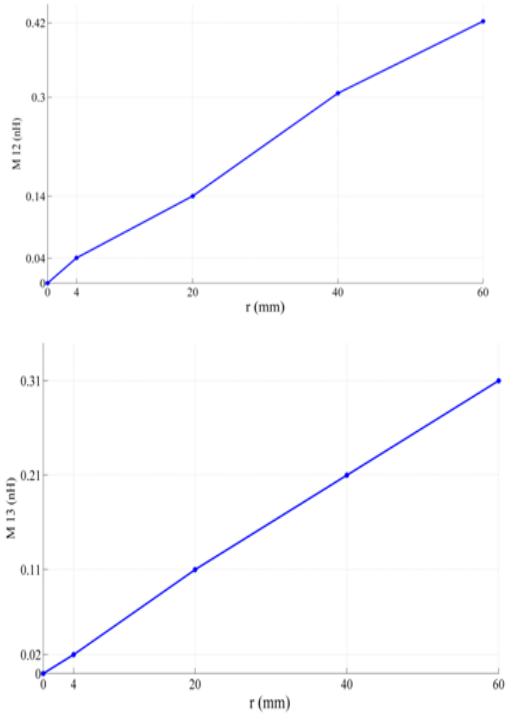

Figure 10. Mutual inductance graph of the first winding for two and three winding

In Figure 10, the mutual inductance graph of the first winding from the flux generated by four, five and six winding M_{14} - M_{15} - M_{16} curve according to r values was drawn with Matlab.

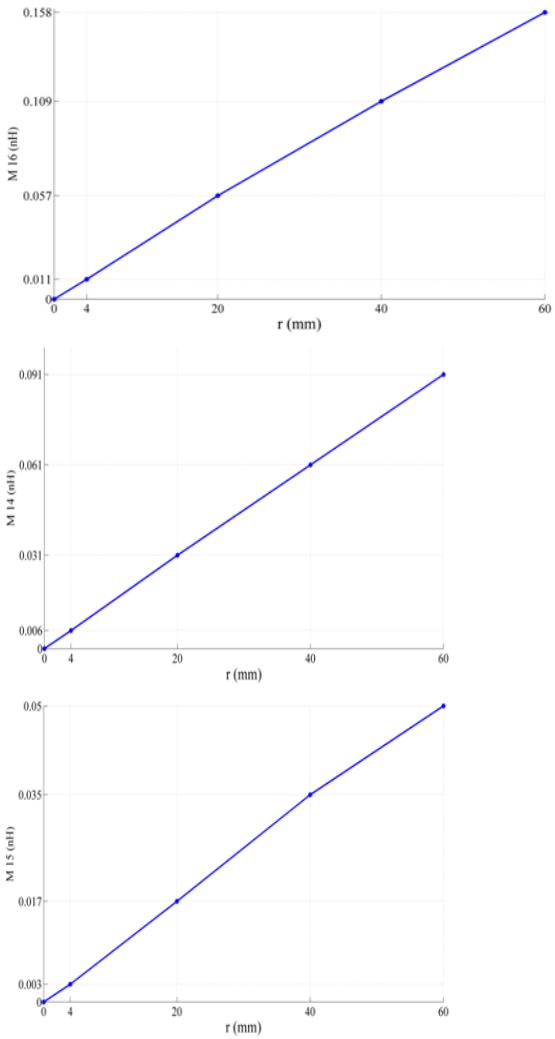

Figure 11. Mutual inductance graph of the first winding for four, five and six winding

As can be seen in Figure 10 and 11, common inductance values also increase as the radius length of the spherical motor increases. Each winding inductance change was examined to be able to estimate inductance values of different radius. Equation 9 was used for the calculation of self inductance coefficients. Common inductance coefficients based on winding numbers are given in Table 4.

Table 4. Function coefficients according to the number of winding

Number of winding	F(x)	Mutual inductance
2	$p_1 = -2{,}132 \times 10^{-6}$ $p_2 = 1{,}936 \times 10^{-4}$ $p_3 = 0{,}002648$ $p_4 = 0{,}02715$	M_{12}
3	$p_1 = 3{,}836 \times 10^{-7}$ $p_2 = -4{,}653 \times 10^{-5}$ $p_3 = 0{,}006783$ $p_4 = -0{,}005211$	M_{13}
4	$p_1 = 8{,}172 \times 10^{-8}$ $p_2 = -8{,}807 \times 10^{-6}$ $p_3 = 0{,}001765$ $p_4 = -0{,}0005226$	M_{14}
5	$p_1 = -3{,}757 \times 10^{-8}$ $p_2 = 1{,}884 \times 10^{-6}$ $p_3 = 0{,}0008672$ $p_4 = 0{,}0001036$	M_{15}
6	$p_1 = 7{,}155 \times 10^{-8}$ $p_2 = -1{,}246 \times 10^{-5}$ $p_3 = 0{,}003157$ $p_4 = -0{,}001135$	M_{16}

4. CONCLUSION

In this study, the numerical analysis of the 3-winding 2-pole spherical motor was carried out with Ansys Maxwell using the finite element method. Spherical structure was determined for the effective location of the windings. In addition, to examine the control and reaction time, inductance changes according to the number of winding and winding radius of the spherical motor to be designed were calculated. Inductance value increased as the winding radius increased. According to these simulation results, and by considering the physical limitations of the motor and the radius of the magnet to be used as rotor, a spherical motor with three winding was applied. The stator windings were designed in a spherical manner, thus the rotor was surrounded and the existing space was used effectively. Static magnetic analysis of spherical motor with permanent magnet rotor was performed. It was found that torque increases as magnet flux increases. This increase is proportional to the increase in Br. The best performance for air core spherical motor model was seen in N52 magnet type. Choosing this magnet and characteristics with high Cuire temperature values (M, SH and UH) can increase production costs.

With the change of size (scale change) in the analyzed spherical motor, the torque increases, but the torque density decreases. Future studies can focus on the open or close cycle dynamic control of the spherical actuator and numerical analysis of torque changes can be conducted by adding soft iron.

DECLARATION OF ETHICAL STANDARDS

The authors of this article declare that the materials and methods used in this study do not require ethical committee permission and/or legal-special permission.

REFERENCES

[1] Bai S., Li X. and Angeles J., "A review of spherical motion generation using either spherical parallel manipulators or spherical motors", ***Mechanism and Machine Theory***, 140: 377-388, (2019).

[2] He J., Fan X., Mu J., Wang C., Qian J., Li X. and Chou X., "3D full-space triboelectric-electromagnetic hybrid nanogenerator for high-efficient mechanical energy harvesting in vibration system", ***Energy***, 116871, (2020).

[3] Li X., Liu J., Chen W. and Bai S., "Integrated design, modeling and analysis of a novel spherical motion generator driven by electromagnetic principle", ***Robotics and Autonomous Systems***, 106: 69-81, (2018).

[4] Xia C., Li H. and Shi T., "3-D magnetic field and torque analysis of a novel Halbach array permanent-magnet spherical motor", ***IEEE Transactions on Magnetics***, 44(8): 2016-2020, (2008).

[5] Li H. and Li T." "End-effect magnetic field analysis of the Halbach array permanent magnet spherical motor", ***IEEE Transactions on Magnetics***, 54(4): 1-9, (2018).

[6] Li Z. and Wang Y., "Finite element analysis and structural optimization of a permanent magnet spherical actuator", ***Elektronika ir Elektrotechnika***, 114(8): 67-72, (2011).

[7] Wang W., Wang J., Jewell, G. W. and Howe D., "Design and control of a novel spherical permanent magnet actuator with three degrees of freedom", ***IEEE/ASME transactions on mechatronics***, 8(4): 457-468, (2003).

[8] Zhang L., Yan L., Chen W. and Liu J., "Current optimization of 3-DOF permanent magnet spherical motor", ***In 2011 6th IEEE Conference on Industrial Electronics and Applications***, Beijing, China, 1111-1116, (2011).

[9] Yan L., Liu Y. and Jiao Z., "Electromagnetic Modeling and Structure Optimization of a Spherical Force Sensing System", ***Sensors***, 19(3): 552, (2019).

[10] Chai F., Gan L., Pei Y. and Yuan L., "Design and Analysis of a Novel Multi-DOF PM Spherical Motor", ***In 2019 22nd International Conference on Electrical Machines and Systems (ICEMS)***, Harbin, China, 1-6, (2019).

[11] Gan L., Pei Y. and Chai F., "Tilting torque calculation of a novel tiered type permanent magnet spherical motor", ***IEEE Transactions on Industrial Electronics***, 67(1): 421-431, (2019).

[12] Park H. J., Lee H. J., Cho S. Y., Ahn H. W., Lee K. D., Park C. Y., and Lee, J., "A performance study on a permanent magnet spherical motor", ***IEEE transactions on magnetics***, 49(5): 2307-2310, (2013).

[13] Wiak S., Napieralska Juszczak E., Ikejiri S., Hirata K. and Maeda S., "Proposal of electromagnetic spherical actuator with 3-DOF", ***COMPEL-The international journal for computation and mathematics in electrical and electronic engineering,*** 29(4): 994-1003, (2010).

[14] Xia C., Song P., Li H., Li B. and Shi T., "Research on torque calculation method of permanent-magnet spherical motor based on the finite-element method", ***IEEE Transactions on Magnetics***, 45(4): 2015-2022, (2009).

[15] Öner Y., "A permanent magnet spherical rotor design and three dimensional static magnetic analysis", ***Sensors and Actuators A: Physical***, 137(2): 200-208, (2007).

[16] Akkaya Oy S., "Robotik sistemler için sabit mıknatıslı küresel motor, sürücü tasarımı ve uygulaması", ***Doktora tezi, Gazi Üniversitesi Fen Bilimleri Enstitüsü***, (2014).

[17] Dalcalı A., "Küresel Eyleyicinin Rotor Mıknatıs Malzemesi Ve Stator Sargı Geometrisinin Eyleyici Torkuna Etkisi", ***Journal Of Engineering Sciences***, 7(1): 145-151, (2019).

[18] Kim H.Y., Kim Y., Gweon D.G. and Jeong J., "Development of a Novel Spherical Actuator with Two Degrees of Freedom", ***Transaction on Magnetics,*** 20(2): 532-540, (2015).

[19] Qian Z., Wang Q., Li G., Guo X., Hu C. and Yan H., "Design and analysis of permanent magnetic spherical motor with cylindrical poles", ***In 2013 International Conference on Electrical Machines and Systems (ICEMS)***, Busan, South Korea, 644-649, (2013).

[20] Kürüm H. Y. and Akın E., " Sabit Mıknatıslı Senkron Motorun Parametre Tespit", ***Fırat Üniversitesi Mühendislik Bilimleri Dergisi***, 30(1): 183-191, (2018).

[21] Shi Y. C., Sun K., Huang L. P. and Li Y., "Online identification of permanent magnet flux based on extended Kalman filter for IPMSM drive with position sensorless control", ***IEEE Trans. Ind. Electron.***, 59(11): 4169–4178, (2012).

[22] Liu Q. and Hameyer K., "A fast online full parameter estimation of a PMSM with sinusoidal signal injection", ***Proc. IEEE Energy Convers. Congr. Expo***, 4091–4096, (2015)

[23] Thierry B., Nicolas L., Babak N. M. and Farid M. T., "Online identification of PMSM parameters: Parameter identifiability and estimator comparative study," ***IEEE Trans. Ind. Appl.***, 47(4): 944–1957, (2011).

[24] Polat M., Öksüztepe E., Kürüm H., "Switched reluctance motor control without position sensor by using data obtained from finite element method in artificial neural network", ***Electrical Engineering*** , 98(1): 43-54, (2016).

[25] Öksüztepe E, Omac Z., Polat M., Celik H., Selcuk A.H., Hasan K. , "Sensorless field oriented control of nonsinusoidal flux-distribution permanent magnet synchronous motor with a FEM based ANN observer", ***Turkish Journal of Electrical Engineering & Computer Sciences*** , 24(4): 2994-3010, (2016).

[26] Cho S., Lee H. J. and Lee, J., "Study on Multi-DOF Actuator for Improving Power Density", ***Energies***, 12(21), 4204, (2019).

[27] Akkaya Oy S. and Gürdal O., "Design and Application of a Two Pole Spherical Permanent Magnet Motor", ***TEM Journal***, 7(1): 53-58, (2018).

[28] Yan L., Chen IM., Lim C.K., Yang G. and Lee KM., "***Torque Modeling. In: Design, Modeling and Experiments of 3-DOF Electromagnetic Spherical Actuators***", Mechanisms and Machine Science, 4. Springer, Dordrecht, (2011).

[29] Yan Liang, Chen I.M., Lim C.K., Yang G., Lin W. and Lee K.M., "Design and analysis of a permanent magnet spherical actuator", ***IEEE/ASME Transactions on mechatronics***, 13(2): 239-248, (2008).

[30] Fenercioğlu A. and Tarımer İ., "Bir manyetik sistemin Maxwell 3D alan simülatörü ile statik manyetik analizinin çözüm süreçleri***", Journal of Selcuk-Technic***, 6(3): 221-240, (2007).

[31] Gürdal O. and Yusuf Ö., "Sabit Mıknatıslı Demir Nüveli Küresel Eyleyicinin Bilgisayar Destekli 3 Boyutlu Statik Manyetik Analizi Ve Uygulaması", ***Gazi Üniversitesi Mühendislik-Mimarlık Fakültesi Dergisi***, 20(4): 433-442, (2005).

[32] Wang J., Jewell G.W. and Howe D., " Analysis, design and control of a novel spherical permanent-magnet actuator", ***IEE Proc.-Electr. Power Appl.***, 145(1): 61-71, (1998).

[33] Tarimer İ. and Dalcali A., "Effects of Permanent Magnets on Torque and Power Density of Spherical Motors", ***TEM Technics Technologies Education Management***, 10(2): 144-149, (2015).

[34] https://www.arnoldmagnetics.com/products/neodymium-iron-boron-magnets/, online aviable:12.07.2019

[35] Gürdal O., "***Elektromanyetik Alan Teorisi",*** Seçkin Yayıncılık, Ankara, (2007).